

Article

Crashworthiness Optimization Method of Ship Structure under Multi-Working Conditions

Weijian Qiu, Kun Liu *, Hwei Liu, Shuai Zong, Jiaxia Wang and Zhenguo Gao

School of Naval Architecture and Ocean Engineering, Jiangsu University of Science and Technology, Zhenjiang 212100, China; 15751774907@163.com (W.Q.); wssls1sw1@163.com (H.L.); 220110101103@stu.just.edu.cn (S.Z.); jxwang66@yeah.net (J.W.); zhenguo.gao@just.edu.cn (Z.G.)

* Correspondence: kunliu@just.edu.cn; Tel.: +86-135-1169-2085; Fax: +86-0511-8444-6543

Abstract: Numerous collision conditions can occur during ship operations, resulting in various consequences that require specific consideration for optimizing crashworthiness design. Existing studies have investigated crashworthiness design in ship structures; however, they often focus on single working conditions and do not comprehensively consider the diverse scenarios encountered during ship operations. To overcome this drawback, this paper proposes a novel method that addresses multi-working conditions and combines orthogonal testing with a backpropagation neural network (BPNN) to establish an efficient surrogate model for collision optimization. The accuracy of the BPNN was improved by introducing the genetic algorithm and Adam algorithm. The technique for order preference by similarity to ideal solution (TOPSIS) is introduced to formulate a multi-working condition optimization function. The crashworthiness of the ship structure is optimized using the sparrow search algorithm (SSA) while considering the constraint of lightweight design. The results demonstrate a substantial reduction in the objective functions for the optimized collision conditions. Moreover, the BPNN predicted values are in good agreement with the finite element simulation results, affirming the effectiveness of the proposed method in improving the crashworthiness of the ship structure and providing valuable guidance for engineering design.

Keywords: ship collision; crashworthiness optimization; surrogate model; multi-working conditions



Citation: Qiu, W.; Liu, K.; Liu, H.; Zong, S.; Wang, J.; Gao, Z. Crashworthiness Optimization Method of Ship Structure under Multi-Working Conditions. *J. Mar. Sci. Eng.* **2023**, *11*, 1335. <https://doi.org/10.3390/jmse11071335>

Academic Editor: Joško Parunov

Received: 31 May 2023

Revised: 27 June 2023

Accepted: 29 June 2023

Published: 30 June 2023



Copyright: © 2023 by the authors. Licensee MDPI, Basel, Switzerland. This article is an open access article distributed under the terms and conditions of the Creative Commons Attribution (CC BY) license (<https://creativecommons.org/licenses/by/4.0/>).

1. Introduction

With the rapid development of the shipping industry, the number of ships sailing at sea is increasing, leading to a rise in ship accidents. In-depth research on ship collision and crashworthiness optimization is necessary to reduce the losses caused by collision accidents and ensure safe navigation at sea. However, the optimization design of ship structures involves finding the optimal solution in a complex and vast search space, which cannot be completed in a short time using traditional optimization methods and may result in search results exploding. Thus, finding efficient intelligent optimization algorithms for engineering optimization problems with high nonlinearity, constraint, and modeling complexity has become a significant research area in related disciplines [1]. Since engineering optimization is typically accompanied by a large number of finite element calculations, the direct application of intelligent optimization algorithms to solve such problems inevitably requires a substantial amount of calculation time. At this point, a surrogate model can be employed to approximate the output of the original model, thereby reducing computational costs. The surrogate model can rapidly predict system responses or evaluate design performance based on input design variables [2,3]. According to the literature [4], compared to the real value, the error rate using the surrogate model is only 1%. These models include the response surface model (RSM), Kriging model, radial basis function (RBF), and BP neural network, all of which have been applied in structure design [5–8].

Currently, the commonly adopted approach is to integrate surrogate models with optimization algorithms. Lin et al. [9] used the twin-stern fin-fishing vessel as the research

object, constructed the sample set of the Kriging model by optimal Latin hypercube sampling (OLHS), and applied the multi-objective evolutionary algorithm (NSGA-II) to achieve the minimum resistance design of the fishing vessel. Prebeg et al. [10] established the surrogate model of tanker crashworthiness with the ultimate strength of the hull girder and ship crashworthiness quality measures as optimization objectives. Through multi-objective optimization, the safety of the structure was improved. Chen et al. [11] combined the adaptive RSM with a multi-objective genetic algorithm to investigate the dynamic response and design optimization of sandwich plates with layered gradients. It can be observed that introducing surrogate models into intelligent optimization algorithms to replace finite element simulation calculations in the optimization process can significantly enhance the optimization efficiency of intelligent optimization algorithms.

Furthermore, for such multi-objective optimization problems, it is worth discussing how to handle conflicts among optimization objectives. Some scholars have adopted the Pareto concept in addressing this issue, which can effectively identify better trade-off solutions in the solution space [12–14]. There are also scholars who have directly optimized all the optimization objectives using a weighted sum method [15,16]. This method, compared to the former one, is simpler and more intuitive in terms of methodology. It also allows for the convenient adjustment of the weights assigned to each optimization objective. However, it is only suitable for problems with lower complexity. When there are multiple conflicts among the optimization objectives, the adoption of the Pareto concept should be considered.

It should be noted that due to the inherent complexity and challenges associated with ship collision issues, current research on optimizing ship structural crashworthiness primarily focuses on a single specific working condition. Compared to other domains, there is relatively limited research on optimizing the structural crashworthiness of ships under multiple working conditions [17–19]. In fact, ship structure design often needs to balance the crashworthiness requirements imposed by various working conditions. When only conducting crashworthiness optimization designs for individual working conditions, conflicts can arise between these conditions. This is because, with identical design variables for the ship structure, the structural damage, deformation, collision forces, and energy absorption differ among these working conditions. While it is possible to demonstrate through verification that the optimization results for one working condition also meet the design requirements for other conditions, this is not the most effective method, especially when two working conditions significantly impact the optimization results.

Therefore, to address the crashworthiness requirements of ship structures under various collision conditions, this paper proposes a multi-working condition crashworthiness optimization method for ship structures based on BPNN, TOPSIS, and SSA (BP-TSSA). To address the issue of insufficient accuracy in traditional BPNN, an improved approach is proposed by incorporating the genetic algorithm (GA) and Adam algorithm to establish a high-precision crashworthiness optimization surrogate model. Different collision positions are selected to carry out multi-working condition crashworthiness optimization analysis on the structural areas mainly concerned by the struck ship, so as to realize the comprehensive optimization effect of multi-working conditions, multi-parameters, and multi-objectives, which can effectively support the engineering design.

It is worth noting that this method still has certain limitations. While it can address crashworthiness optimization problems under different collision locations, angles, and velocities, it cannot simultaneously consider factors such as collision location, collision angle, and collision velocity. Further research is therefore needed to address this limitation.

This paper is organized as follows. Following this introduction, the optimization method, including the improvement of the neural network surrogate model, optimization algorithm, and multi-working optimization functions, is introduced in Section 2. Section 3 describes the application examples of the crashworthiness optimization of the selected structure under two different collision conditions based on BP-TSSA. The discussion of the results is presented in Section 4, and major conclusions are drawn in Section 5.

2. Multi-Working Condition Optimization Method

This paper considers the randomness of hull collision positions in ship collision accidents by selecting two different positions located at the stern of a ship for collision analysis. The first position is at the center of the plate and the second position is at the intersection of the plate and frame, named Condition 1 and Condition 2, respectively (as illustrated in Figure 1). The crashworthiness optimization design process under multi-working conditions is presented in Figure 2. The employed optimization method is BP-TSSA, which utilizes BPNN to establish a collision-resistant optimization surrogate model. Subsequently, the TOPSIS is employed to construct a multi-working condition optimization function for SSA. Finally, the SSA is utilized to optimize the function. The primary optimization process is as follows:

1. Definition of the design variables, constraints, and objective function of the optimization problem and establishment of the mathematical model;
2. Utilization of orthogonal design to construct test sample points in the design domain, with each sample point corresponding to one numerical simulation case. The structural responses corresponding to each sample point are obtained through finite element analysis;
3. Normalization of the orthogonal table and finite element simulation results and input into BP neural network (for different collision conditions, corresponding BPNN is established, respectively);
4. SSA optimization to obtain ideal points of each optimization objective under different collision conditions and establish a multi-working condition evaluation function;
5. SSA optimization to obtain the optimal solution that can make each working condition relatively optimal based on the above evaluation function.

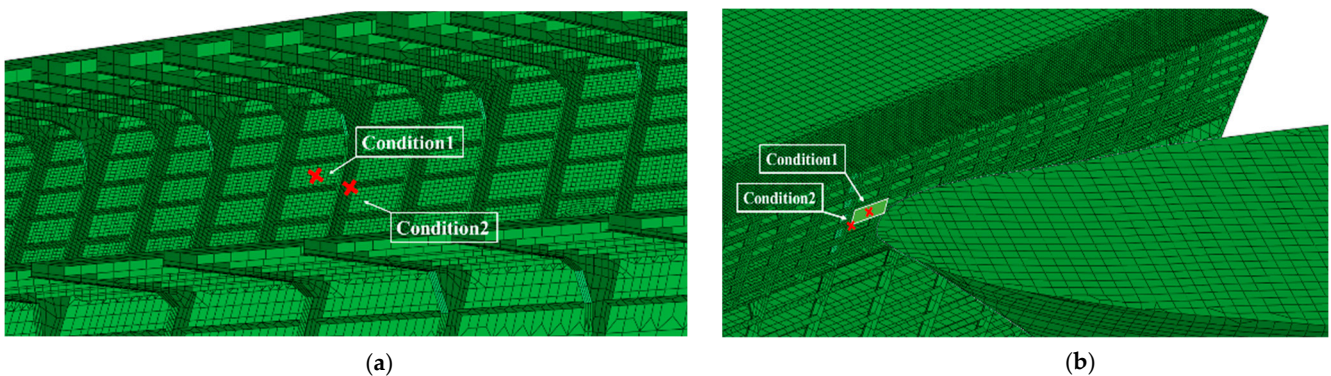


Figure 1. (a) Collision positions from interior perspective; (b) collision positions from exterior perspective.

2.1. Mathematical Model for Crashworthiness Optimization

2.1.1. Single Working Condition

For conventional single-working condition optimization problems, what needs to be established is a multi-objective optimization function. Multi-objective optimization design can achieve a balance in overall design performance. For instance, optimization objectives such as weight, energy absorption, and deformation are simultaneously considered, aiming to attain a design solution that can optimize these objectives in a relative sense. Mathematically, multi-objective optimization problems can be formulated as follows [20]:

$$\begin{cases} \min & f(\mathbf{X}) = f(x_1, x_2, \dots, x_n) \\ \text{s.t.} & g_j(\mathbf{X}) \leq 0 & j = 1, 2, \dots, J \\ & x_{i,\min} \leq x_i \leq x_{i,\max} & i = 1, 2, 3, \dots, n \end{cases} \quad (1)$$

where $\mathbf{X} = (x_1, x_2, \dots, x_n)$ is a design variable, $f(\mathbf{X})$ is a multi-objective function, J is the total number of constraints, $g_j(\mathbf{X})$ is the j th constraints, x_i is the i th design variable, and $x_{i,\max}$ and $x_{i,\min}$ are the upper and lower limits, respectively.

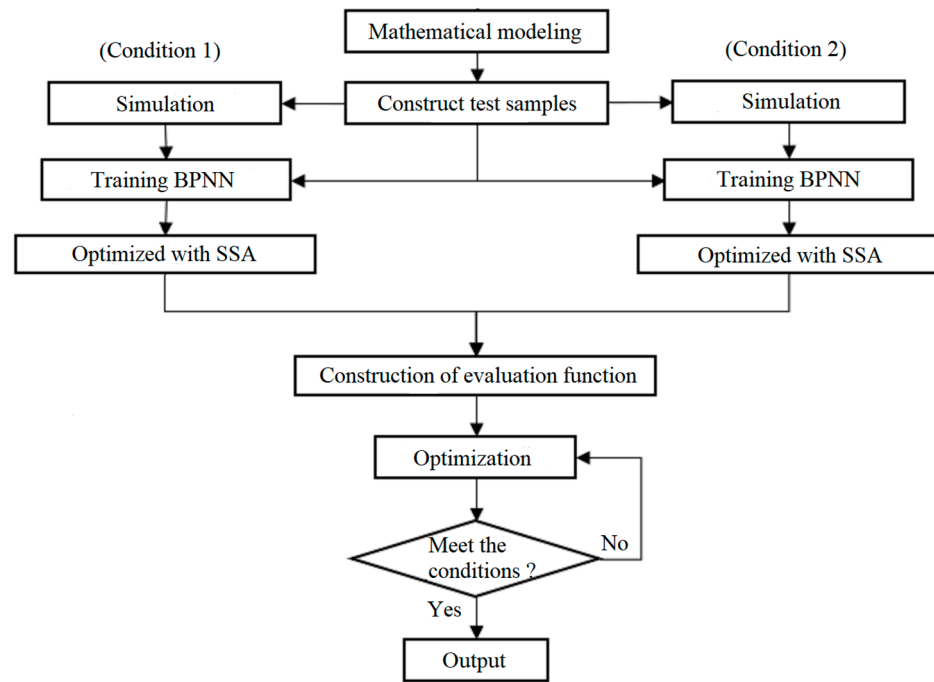


Figure 2. Crashworthiness optimization process.

In this paper, the linear weighting method of constructing the evaluation function is used to address multi-objective optimization problems. The linear weighting method aims to transform a multi-objective optimization problem into a single-objective optimization problem. This is accomplished by assigning weight coefficients to each objective based on their relative importance in the optimization problem. The evaluation function utilizing the linear weighting method can be expressed as follows [21]:

$$F(\mathbf{X}) = \sum_{i=1}^n \alpha_i f_i(\mathbf{X}) \tag{2}$$

where α_i is the weight coefficient of i th optimization objective. Each weight coefficient is between 0 and 1, and the sum of all the ownership weight coefficients is equal to 1. $f_i(\mathbf{X})$ is the i th optimization objective after normalization using Equation (3) [22].

$$Objective_{membership} = \frac{Objective_{value} - Objective_{min}}{Objective_{max} - Objective_{min}} \tag{3}$$

where $Objective_{value}$ is the normalized value of each index and $Objective_{max}$ and $Objective_{min}$ are the maximum and minimum values corresponding to each indicator in the orthogonal design sample. It should be noted that $Objective_{max}$ and $Objective_{min}$ do not represent optimized maximum and minimum values in the traditional sense, as they are only used for data normalization. They can be found directly in the orthogonal design sample.

In multi-objective optimization problems, certain objectives require maximization, while others require minimization. It is known that the maximum value of a function is equivalent to the minimum value of its negative counterpart. This paper incorporates this concept to enhance the multi-objective optimization function:

$$F(\mathbf{X}) = \sum_{i=1}^n \alpha_i f_i(\mathbf{X}) - \sum_{j=n+1}^m \alpha_j f_j(\mathbf{X}) \tag{4}$$

where α_i is the optimization objective weight coefficient that requires the minimum value and α_j is the optimization objective weight coefficient that requires the maximum value.

This paper considers several indicators that can comprehensively evaluate the crashworthiness of hull structures as optimization objectives, including weight, peak collision force, collision depth, and plastic energy absorption. Weight is an indispensable factor for realizing ship lightweight. Collision depth, collision force, and plastic energy absorption can, to a certain extent, reflect the crashworthiness of the structure. Regarding the collision depth, this paper primarily focuses on the plastic deformation of the struck ship structure. Generally, the greater the collision depth, the more significant the kinetic energy loss of the struck ship. The lost kinetic energy will be transformed into the plastic energy absorption of the struck ship structure during the collision process, hence increasing the plastic energy absorption of the struck ship structure. In order to minimize damage to people and cargo, it is essential to reduce the plastic deformation of the collision zone of the crashed ship as much as possible or to maintain the overall damage deformation within a narrow range, thus enhancing the safety of the structure. Collision force signifies the hull structure’s ability to resist collision loads. In this paper’s crashworthiness optimization research, the peak value of the collision force in the collision process is of primary concern. The higher the peak value, the more robust the hull structure’s ability to resist collision loads.

It is evident that the following relationships exist among the four comprehensive crashworthiness indicators mentioned above:

1. Increasing the structural size can significantly enhance the crashworthiness of the ship but it will also increase the total weight of the ship;
2. Blindly pursuing structural lightweight can lead to a decrease in the crashworthiness of the ship. Specifically, the peak value of the collision force decreases and the collision depth increases, which is detrimental to the safety of the structure;
3. The coupling relationship between collision depth and plastic energy absorption is strong, considering both the collision depth and plastic energy absorption can effectively reduce the collision depth or collision depth range.

Equation (5) represents the multi-objective evaluation function of ship structure crashworthiness optimization under a single working condition. By assigning weight coefficients to each crashworthiness index and transforming it into the index’s minimum value, the conflict between the indexes can be effectively resolved:

$$F = \alpha_M \cdot f(M) + \alpha_D \cdot f(D) - \alpha_P \cdot f(P) + \alpha_E \cdot f(E) \tag{5}$$

where the dimensionless quantity, $f()$, is obtained by normalizing each crashworthiness index using the formula presented in Equation (3). α_M , α_D , α_P , and α_E are the weight coefficients of weight, collision depth, collision force, and energy absorption, respectively. The optimal crashworthiness of a structure is achieved when its weight is minimized, collision force is maximized, and collision depth and plastic energy absorption are minimized. However, the coupling relationship between collision depth and energy absorption should also be considered to avoid overemphasis on optimization. Setting the weight coefficient too high may result in over-optimization, while setting it too low may not effectively improve the crashworthiness of the structure. This paper takes into account the relationships and relative importance of the four crashworthiness indicators and proposes the weight coefficients denoted as: $\alpha_M = 0.5$, $\alpha_D = 0.15$, $\alpha_P = 0.2$, and $\alpha_E = 0.15$, which achieves a balanced optimization.

When the optimization problem has constraints, the constrained problem is transformed into an unconstrained problem through the penalty function [23]:

$$F(\mathbf{X}) = \begin{cases} F(\mathbf{X}) & \text{if } \mathbf{X} \in K \\ 1 & \text{if } \mathbf{X} \notin K \end{cases} \tag{6}$$

where \mathbf{X} is the design variable and K is the feasible region of the optimization problem.

2.1.2. Multi-Working Conditions

For the multi-working condition crashworthiness optimization problem addressed in this paper, it is imperative to not only establish a reasonable multi-objective evaluation function for each working condition but also develop a multi-working condition evaluation function to achieve relatively optimal performance across all conditions.

Technique for Order Preference by Similarity to Ideal Solution (TOPSIS), also known as the distance method of superior and inferior solutions, is a multi-objective decision-making method initially proposed by C.L. Hwang and K. Yoon [24]. The fundamental principle behind TOPSIS is to rank alternatives by calculating their distances to both the ideal and worst solutions. By determining the closest proximity to the ideal solution and the farthest distance from the worst solution, the method identifies the best alternative. For multi-objective optimization problems, if it is possible to assign a value f_i^* to each optimization objective such that $f_i^* \leq \min f_i(\mathbf{X})$ holds, then these values are referred to as "ideal points" for these optimization objectives.

In this paper, when dealing with multi-working condition optimization problems, the ideal point for the i th optimization objective is taken as the minimum value achieved when optimizing that objective function independently. Therefore, the multi-working condition optimization problem can be transformed into finding a solution that minimizes the weighted sum of distances between each optimization objective and its corresponding minimum value across all working conditions. This can be expressed as follows:

$$F(\mathbf{X}) = \sum_{i=1}^n \omega_i \cdot [W_1 \cdot |f_{i1}(\mathbf{X}) - f_{i1}^*(\mathbf{X})| + W_2 \cdot |f_{i2}(\mathbf{X}) - f_{i2}^*(\mathbf{X})|] \quad (7)$$

where n is the number of optimization objectives, ω_i is the weighting coefficient for each optimization objective, and $|f_{i1}(\mathbf{X}) - f_{i1}^*(\mathbf{X})|$ and $|f_{i2}(\mathbf{X}) - f_{i2}^*(\mathbf{X})|$ are the distances between each optimization objective and its corresponding ideal point under two different collision conditions, respectively. Here, $f_{i1}(\mathbf{X})$, $f_{i1}^*(\mathbf{X})$, $f_{i2}(\mathbf{X})$, and $f_{i2}^*(\mathbf{X})$ are calculated using the normalization function described earlier in the text. W_1 and W_2 are the weighting coefficients for the two collision conditions. This paper assumes that both collision conditions are equally important; thus, W_1 and W_2 are both set to 0.5.

2.2. BPNN Surrogate Model

The surrogate model serves as a means of emulating the correlation between input variables and output responses within the optimization problem. Typically, the surrogate model is established by either defining the input and output of the model with or without prior knowledge of the internal computation process. The selection of initial sample points determines the amount of original information captured within the model, whereby a greater number of initial sample points results in a higher degree of original information; however, this comes at the expense of increased computational time. To mitigate this, this present paper employs a scientifically rigorous experimental design method (orthogonal design) to systematically arrange tests, thereby reducing the number of tests required and shortening the test cycle [25]. To eliminate the influence of the different dimensions and units of sampling data on the analysis results, all the sample data are normalized to the range of 0~1.

In this paper, BPNN [26] is used as the surrogate model of the optimization problem, and orthogonal design is used to provide initial sample points for the surrogate model. Figure 3 shows the three-layer structure of BPNN. Specifically, the input layer comprises n nodes, the hidden layer contains g nodes, and the output layer encompasses m nodes. The connection weights between nodes are denoted by ω , while θ represents the threshold that affects the nodes.

The training algorithm used for the BPNN is the error backpropagation algorithm, commonly known as the BP algorithm. The objective of backpropagation is to minimize the error during the training process by estimating the error before the output layer using the output error and subsequently estimating the error of the previous layer. This process

involves gradually transmitting the error from the output layer to the input layer in the opposite direction of input transmission while gradually updating the weights to approximate the expected output.

However, the BPNN still has the following two shortcomings:

1. It is difficult to determine the initial weights and thresholds of the network, and it is prone to get stuck in a local optimum;
2. The fixed learning rate can result in slow network convergence or system instability.

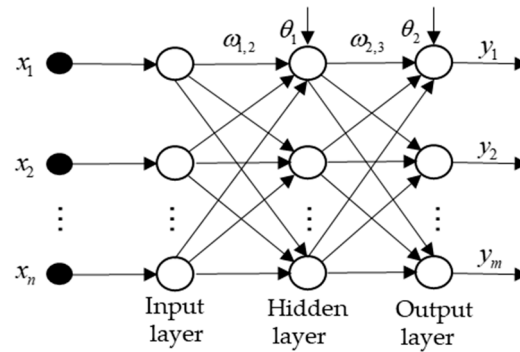


Figure 3. Three-layer BP neural network.

To overcome these limitations, this paper employs both the genetic algorithm and the Adam algorithm to enhance the performance of the BPNN.

2.2.1. Modification of BPNN Surrogate Model

The genetic algorithm was initially proposed by Holland in the 1970s [27]. In this paper, the genetic algorithm is utilized to optimize the initial parameters (weights and thresholds) of the BP neural network (BPNN). The optimization process involves the following steps:

1. Converting the parameters to be optimized into chromosomes using real number coding;
2. Using the network error as the objective function and the reciprocal of the error as the fitness function to evaluate the adaptability of the chromosomes;
3. Performing genetic operations such as selection, crossover, and mutation on the current population to update the population and select the optimal chromosome;
4. Outputting the optimal combination of initial parameters that minimize the error at the end of the iteration.

The fitness function of the genetic algorithm is given as:

$$F = \frac{1}{E + \lambda} \tag{8}$$

where E is the loss function (error) and λ is a constant close to 0. When F exceeds a predetermined upper limit, it is truncated to that upper limit to prevent the influence of F approaching infinity on the optimization process.

The Adam algorithm, introduced by Kingma [28], derives its name from “adaptive moment estimation”. It is a network learning algorithm that accelerates network convergence by adaptively adjusting the learning rate and is capable of finding smaller errors than the traditional gradient descent method. As such, it can be used to train BPNN. The Adam algorithm introduces the concept of momentum, where first-order momentum suppresses oscillations in the network training process of the gradient descent method, while second-order momentum provides different learning rates for the network at different stages of training, balancing the adjustment of each parameter update. The formulas for first-order momentum and second-order momentum are given by Equations (9) and (10), respectively:

$$m_t = \beta_1 \cdot m_{t-1} + (1 - \beta_1) \cdot dk \tag{9}$$

$$v_t = \beta_2 \cdot v_{t-1} + (1 - \beta_2) \cdot dk^2 \tag{10}$$

where t is the current iteration number and dk is the gradient of the error function with respect to the weight or threshold. m and v are gradient first-order momentum and second-order momentum, respectively. β_1 and β_2 are the exponential decay rates of m and v , respectively, which are used to emphasize the gradients closer to the current moment, meaning that the impact of gradients decreases as they move farther away from the current moment.

By combining the first-order and second-order momentum of the gradient, the parameter change can be calculated under the current learning rate, and the parameters can be updated accordingly:

$$\eta_t = \alpha \cdot \frac{1}{\sqrt{v_t} + \delta} \tag{11}$$

$$\omega_t = \omega_{t-1} - \eta_t \cdot m_t \tag{12}$$

$$\theta_t = \theta_{t-1} - \eta_t \cdot m_t \tag{13}$$

where α is the initial learning rate, η_t is the learning rate of the current parameter calculated, and δ is a constant used to prevent the denominator from being 0. ω_t and θ_t are the updated weight and threshold values, respectively.

The principles of the Adam algorithm indicate that it utilizes the first-order momentum of the gradient to regulate the direction of model updates and the second-order momentum of the gradient to dynamically adjust the learning rate. This approach not only avoids network oscillation during training but also allocates distinct learning rates to different parameters at various stages, significantly simplifying the process of model adjustment.

The procedures of training BPNN with the Adam algorithm are as follows:

1. Randomly initialize network parameters (weights and thresholds);
2. Combine the sample data with the initialized parameters to calculate the output of each layer in the network;
3. Calculate the gradients by taking derivatives of the loss function with respect to the parameters;
4. Update the first and second moment estimates of the gradient and update the learning rate and parameters accordingly;
5. If the desired number of training iterations is reached, terminate the training process; otherwise, repeat steps (2) to (4).

2.2.2. Parameter Settings for BPNN Surrogate Model

The parameter settings for BPNN include determining the network structure and the algorithm parameters.

While having more hidden layers is commonly believed to improve the model's accuracy, it also increases its complexity. This paper adopts a three-layer backpropagation neural network with only one hidden layer as the primary approach, and the number of nodes in the hidden layer is determined by Kolmogorov's theorem. According to Kolmogorov's theorem, the network model achieves optimal accuracy when the relationship between the m nodes of the input layer and the n nodes of the hidden layer is approximately $n = 2m + 1$.

To introduce nonlinear characteristics to the backpropagation neural network, the Sigmoid function is selected as the activation function. The Sigmoid function can smoothly map the real field to a range of 0 to 1, and its functional form is given by:

$$f(x) = \frac{1}{1 + e^{-x}} \tag{14}$$

The mean square error function (MSE) is utilized as the loss function to assess the discrepancy between the predicted value and the true value of the network model. The loss value is also referred to as the mean square error, and the smaller the value, the higher the model's accuracy. The formula for the mean square error function is:

$$MSE = \frac{1}{n} \sum_{i=1}^n |y - y'|^2 \tag{15}$$

where n is the total number of data output from the output layer, y is the true value, and y' is the predicted value.

BPNN is trained based on normalized sample data, and the preset parameters for the algorithm are set for BPNN in this section. Specifically, the genetic algorithm employs a population size of 50 and performs 5000 iterations, while the Adam algorithm is trained for 8000 iterations with an initial learning rate α of 0.001. Additionally, the first-order momentum exponential decay rate of the gradient β_1 is 0.9, the second-order momentum exponential decay rate of the gradient β_2 is 0.99, and the δ value is set to 10^{-8} .

2.3. Improved Sparrow Search Algorithm

As one of the swarm intelligence optimization algorithms, the sparrow search algorithm shares the same optimization mechanism as other algorithms in this category [29]. It relies on a population-based search, where each individual in the population represents a set of design schemes for the optimization problem at hand. The sparrow search algorithm achieves optimization by imitating the behavior of sparrows, including foraging, anti-predation, and investigation.

In the sparrow search algorithm, the population of sparrows can be divided into two main categories: explorers and followers. Explorers are responsible for locating food sources and providing suitable foraging areas for the followers. The fitness value of a sparrow represents the quality of its current location. When a follower discovers a better position, it competes with the explorers and brings along its own explorers, resulting in dynamic changes within the population.

To mitigate the risk of getting trapped in local optima, the population also includes scout sparrows. These scouts compare their fitness with the sparrows occupying the optimal position, thereby reducing the likelihood of falling into local optima.

Although the sparrow search algorithm generally yields favorable results in addressing most function optimization problems, a study by Yan et al. [30] revealed that the algorithm can still encounter challenges when dealing with complex multi-peak problems. Therefore, there is a need for further enhancements to the sparrow search algorithm.

Opposition-based learning (OBL) is a population generation strategy introduced by Tizhoosh et al. [31] in 2005, specifically designed for swarm intelligence optimization algorithms. OBL aims to enhance the uniformity of the population distribution through an opposite search approach. This strategy effectively addresses the limitations of swarm intelligence optimization algorithms that may suffer from insufficient population diversity due to the random generation of initial populations.

In OBL, if the j -dimensional position information of the i th sparrow in the new population is represented by $x_{i,j}$, the corresponding update formula for the opposite position information $x_{i,j}^*$ can be expressed as follows:

$$x_{i,j}^* = k(lb_j + ub_j) - x_{i,j} \tag{16}$$

where ub_j and lb_j are the upper and lower bounds of the j -dimensional design domain, respectively, and k is a random number between 0 and 1.

To enhance the population diversity in the algorithm, the search strategy of the Bird Swarm algorithm [32] is employed to enhance the location update formula for both explorers and followers. The position update for explorers is based on a Gaussian random distribution. The update formula for follower locations is adjusted to increase the likelihood

of approaching the current optimal explorers. This modification is performed with a certain probability:

$$x_{i,j}^{t+1} = \begin{cases} x_{i,j}^t + x_{i,j}^t \cdot p & \text{if } R_2 < ST \\ x_{i,j}^t + Q \cdot L & \text{if } R_2 \geq ST \end{cases} \quad (17)$$

where $x_{i,j}$ is the location information of the i th sparrow in the j dimension and p is Gaussian distribution with a mean value of 0 and standard deviation of 1. R_2 and ST are alarm value and security value, respectively; Q is a random number subject to normal distribution; and L is a matrix of $1 \times d$, in which each element is 1.

$$x_{i,j}^{t+1} = \begin{cases} Q \cdot \exp\left(\frac{x_{worst}^t - x_{i,j}^t}{i^2}\right) & \text{if } i > n/2 \\ x_p^{t+1} + (x_{i,j}^t - x_p^{t+1}) \cdot FL \cdot k & \text{if } i \leq n/2 \end{cases} \quad (18)$$

where n is the total number of sparrows, i is the follower number except the explorer in the sparrow population, x_p is the current position of the optimal explorer, x_{worst} is the worst position among all the current sparrows, Q is a random number subject to normal distribution, k is a random number between 0 and 1, and $FL \in [0, 2]$ is the probability followers approaching the explorer.

Levy flight is a strategy that enhances the local search capability of the algorithm [33]. It is characterized by both small and large step lengths. When the algorithm is searching near the optimal position, the Levy flight strategy effectively prevents it from getting trapped in local optima. Thus, Levy flight can be incorporated into the position update formula for investigators, improving the control parameters of step size, denoted as β and K . A larger step size benefits the global search of the algorithm, while a smaller step size benefits the local search:

$$x_{i,j}^{t+1} = \begin{cases} Levy \cdot x_{best}^t + \beta \cdot |x_{i,j}^t - Levy \cdot x_{best}^t| & \text{if } f_i > f_g \\ x_{i,j}^t + K \cdot \left(\frac{|x_{i,j}^t - x_{worst}^t|}{(f_i - f_w) + \epsilon}\right) & \text{if } f_i = f_g \end{cases} \quad (19)$$

$$\beta = f_g - (f_g - f_w) \cdot \left(\frac{iter_{max} - t}{iter_{max}}\right)^{1.5} \quad (20)$$

$$K = (f_g - f_w) \cdot \exp\left(-20 \cdot \tan\left(\frac{t}{iter_{max}}\right)^2\right) \cdot (2c - 1) \quad (21)$$

$$Levy = 0.01 \cdot \frac{r_1 \cdot \sigma}{|r_2|^{1/\lambda}} \quad (22)$$

$$\sigma = \left\{ \frac{\Gamma(1 + \lambda) \cdot \sin(\pi\lambda/2)}{\Gamma[(1 + \lambda)/2] \cdot \lambda \cdot 2^{(\lambda-1)/2}} \right\}^{1/\lambda} \quad (23)$$

where t is the current iteration number; $iter_{max}$ is the maximum number of iterations; x_{best} is the current optimal location; f_i is the fitness value of the current sparrow; f_g is the fitness value of the current optimal position; f_w is the fitness value of the current worst position; ϵ is a constant used to make the denominator not zero; c is a random number between 0 and 1; Γ is the gamma function; λ is a constant between 0 and 2, generally, 1.5; and r_1 and r_2 are random numbers between 0 and 1.

The main SSA process is as follows:

1. Randomly initialize the sparrow population;
2. Calculate the fitness of each sparrow and sort them in descending order based on their fitness values;
3. Update the location of the explorer and follower sparrows alternately. This step involves adjusting the positions of these sparrows based on specific rules or algorithms;

4. Randomly select investigator sparrows and update their locations using a predefined strategy or method;
5. Check if there is a better position found during the previous steps. If a better position is found, update the optimal position accordingly;
6. Check if the termination condition of the algorithm is satisfied. If it is, output the optimal solution obtained so far. Otherwise, repeat steps (2) to (5) to continue the execution of the algorithm.

3. Example Analysis of Multi-Working Conditions Crashworthiness Optimization

3.1. Ship Collision Scenario and Its Primary Optimization Components

The collision scenario selected for this paper involves the bow of the striking ship colliding with the tail of the struck ship at a collision angle of 150° . Figure 4 illustrates a diagram of the ship collision. The coordinate system's origin for the struck ship is situated at the stern baseline, with the x -axis running from stern to bow, the y -axis running from starboard to port, and the z -axis running from baseline to deck. The coordinate origin for the striking ship is located at the baseline position of the striking ship's stern. When the collision occurs, the striking ship and the struck ship's course align with their respective x -axis coordinates, and there is no rotation.

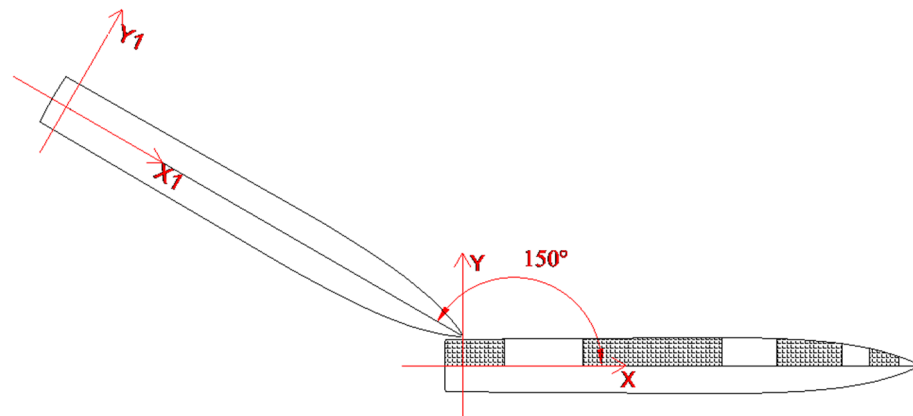


Figure 4. Diagram of ship collision.

To simplify the calculation process and ensure the validity of the results, the relative impact velocity method is used when setting the speed, where the struck ship is assumed to be stationary, and the relative impact velocity of the striking ship is 5 knots. This approach streamlines the calculation process while ensuring the accuracy of the results.

Figure 5 shows the finite element model of the ship, which was established using the ABAQUS finite element software. The collision location is the stern side of the struck ship. Since this paper mainly focuses on investigating the structural response of the collision zone of the struck ship, the striking ship was set as a rigid body, whereas the struck ship was set as a deformable body, with the collision zone of the struck ship meshed. To optimize simulation computation time, the collision region of the struck ship is enhanced with a finer mesh, whereas coarser meshes with a mesh size of 0.25 m are employed for the remaining areas of both the struck and striking ships. Both striking ship and struck ship were modeled with the four-node shell element S4R from the ABAQUS element library. A mesh sensitivity analysis is performed on the collision region of the struck ship to ascertain an appropriate mesh size. Figure 6 demonstrates the collision region models of the struck ship at varying mesh sizes of 0.1 m, 0.05 m, and 0.025 m, respectively.

The collision force curves obtained from the three different mesh sizes mentioned above are shown in Figure 7. It can be observed that these collision force curves exhibit good convergence, with minimal differences in the computed results when using mesh sizes of 0.05 m and 0.025 m. Therefore, for the subsequent analysis, a uniform mesh size of 0.05 m is adopted for the collision region of the struck ship.

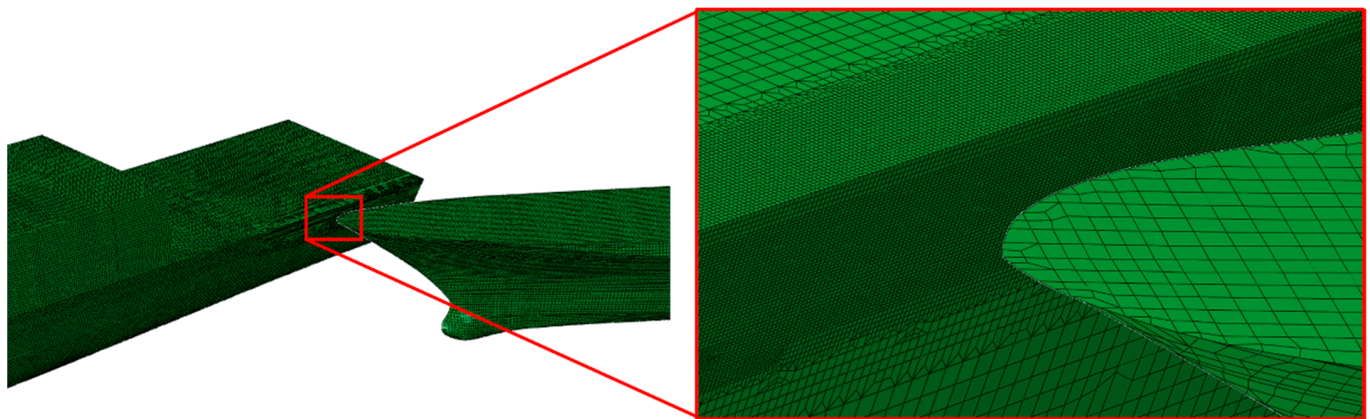


Figure 5. FEM of ship collision.

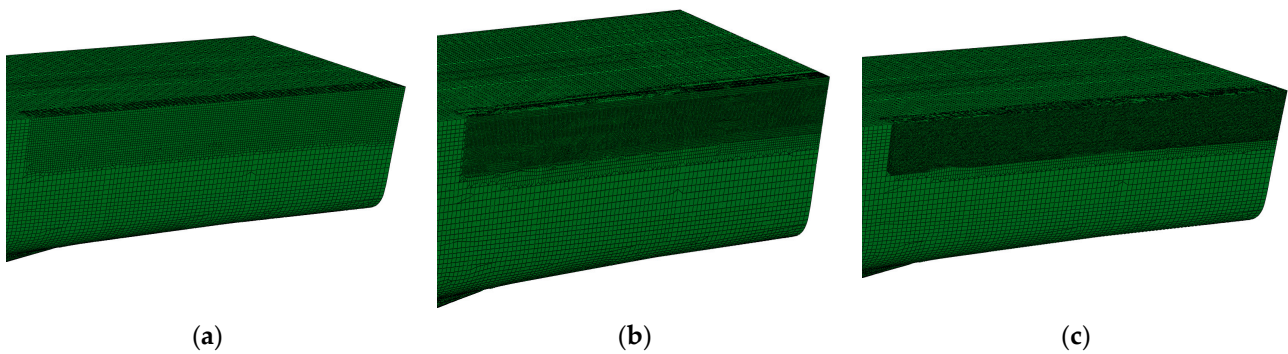


Figure 6. (a) Mesh size of 0.1 m, (b) mesh size of 0.05 m, (c) mesh size of 0.025 m.

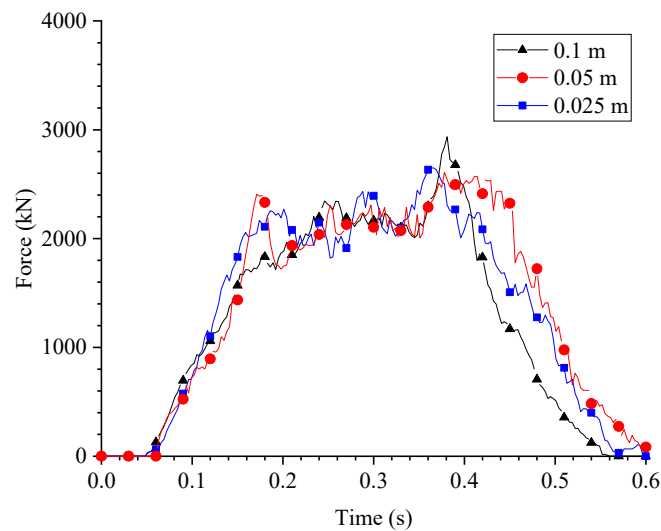


Figure 7. Collision force curves at different mesh sizes.

The primary parameters of both vessels are presented in Table 1, indicating that the striking ship has a total mass of 1000 T and the struck ship has a total mass of 3850 T.

Table 1. Principle parameters of collision ships.

Collision Ships	Total Length/m	Beam Molded/m	Molded Depth/m	Total Mass/T
Struck ship	132.00	16.00	8.60	3850
Striking ship	83.00	9.77	6.68	1000

For the collision simulation, the model uses general contact with both normal and tangential contact attributes. The normal contact attribute is set to hard contact while the tangential contact attribute uses the penalty function method, with a friction coefficient of 0.3. The Cowper-Symonds model, which considers the material’s strain rate sensitivity, is employed as the constitutive model for the hull material [34,35]:

$$\frac{\sigma_d}{\sigma_y} = 1 + \left(\frac{\dot{\epsilon}}{D}\right)^{\frac{1}{q}} \tag{24}$$

where σ_d is dynamic yield stress, σ_y is static yield stress, $\dot{\epsilon}$ is equivalent strain rate, and D and q are constants set to 40.4 and 5, respectively.

To simulate ship collision in a water medium, the impact of water on the collision effect is taken into account by including the attached water mass [36]. In the case of ship–ship collision, the transverse motion mainly affects the struck ship, while the forward and backward motion mainly affects the striking ship. Therefore, this paper only considers the attached water mass of the transverse and the forward–backward motion. Equations (25) and (26) represent the empirical formulas for the added water mass of the struck ship and the striking ship, respectively:

$$m_1 = (0.4 \sim 1.3)m \tag{25}$$

$$m_2 = (0.02 \sim 0.07)m \tag{26}$$

where m is the hull mass. The attached water mass of the struck ship is $0.4 m$ and that of the striking ship is $0.03 m$.

Figure 8 shows the model structure diagram of the collision area of the struck ship. The shell plating and the frame act as the primary energy-absorbing components in this region during an impact load. Therefore, this paper aims to adjust the thickness of the shell plating and the size of the frame web while retaining the original structure of the struck ship.

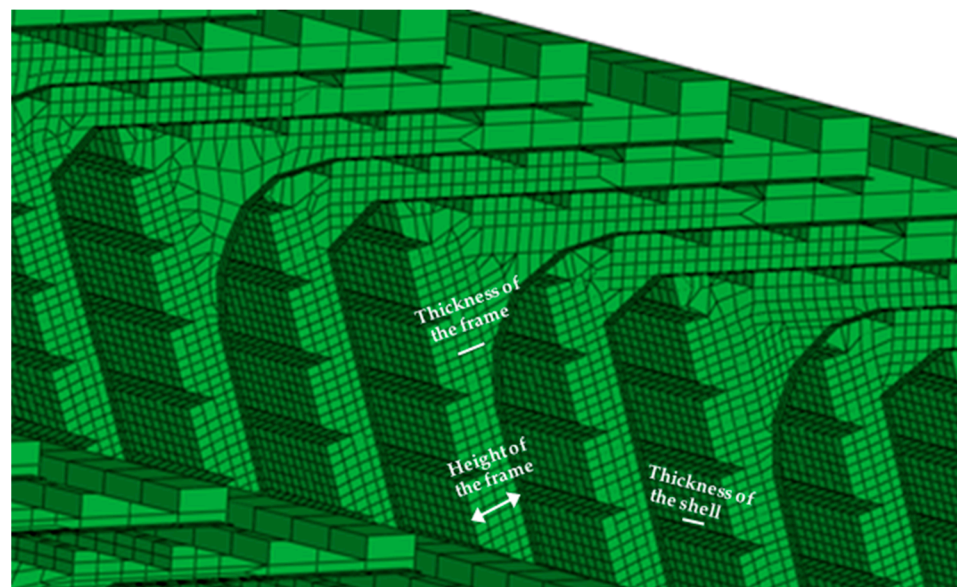


Figure 8. Model structure diagram of collision area.

The thickness of the shell plating and the thickness and height of the frame web are considered design variables, with the original shell plating of the struck ship having a thickness of 13 mm, a frame size of 240 mm × 6 mm/40 mm × 8 mm, and a longitudinal bone size of 100 mm × 7.5 mm. To ensure the rationality of the structure, the design

domain of the shell plating thickness ranges from 13 mm to 16 mm, the design domain of the frame web thickness ranges from 4 mm to 7 mm, and the design domain of the frame web height ranges from 200 mm to 260 mm. The structural weight is considered a constraint condition, and the weight calculated from the 11th sample point in Tables 2 and 3 serves as the threshold that should not be exceeded in a lightweight design. Therefore, its value should be less than or equal to 4860.96 kg to incorporate lightweight design principles.

Table 2. Orthogonal design and finite element simulation results for working condition 1.

Sample Number	Thickness of the Shell Plating/(mm)	Thickness of the Frame Web/(mm)	Height of the Frame Web/(mm)	Weight/(kg)	Peak Collision Force/(N)	Collision Depth/(m)	Plastic Energy Absorption/(J)	Objective Function Value
1	13	4	200	4161.92	2,508,050	0.082	118,796.65	0.357
2	13	5	220	4295.25	2,651,900	0.079	123,713.37	0.368
3	13	6	240	4437.30	2,640,630	0.075	128,236.35	0.416
4	13	7	260	4580.71	2,849,940	0.069	132,640.73	0.365
5	14	4	220	4415.32	2,681,830	0.078	116,599.61	0.378
6	14	5	200	4514.94	2,675,860	0.076	118,022.23	0.411
7	14	6	260	4693.83	2,746,050	0.071	123,799.87	0.441
8	14	7	240	4798.00	2,677,790	0.069	121,210.58	0.480
9	15	4	240	4669.56	2,292,020	0.071	102,084.79	0.486
10	15	5	260	4806.95	2,365,960	0.071	105,583.03	0.537
11	15	6	200	4860.96	2,869,170	0.073	116,529.87	0.469
12	15	7	220	5008.76	2,826,550	0.070	113,533.07	0.507
13	16	4	260	4920.06	2,231,700	0.069	99,321.75	0.583
14	16	5	240	5030.26	2,332,510	0.069	100,145.03	0.610
15	16	6	220	5128.84	2,251,270	0.069	100,168.92	0.677
16	16	7	200	5220.97	2,450,980	0.068	96,076.65	0.631

Table 3. Orthogonal design and finite element simulation results for working condition 2.

Sample Number	Thickness of the Shell Plating/(mm)	Thickness of the Frame Web/(mm)	Height of the Frame Web/(mm)	Weight/(kg)	Peak Collision Force/(N)	Collision Depth/(m)	Plastic Energy Absorption/(J)	Objective Function Value
1	13	4	200	4161.92	2,120,530	0.073	95,290.00	0.381
2	13	5	220	4295.25	3,644,950	0.069	120,226.30	0.292
3	13	6	240	4437.30	3,533,160	0.066	118,995.62	0.336
4	13	7	260	4580.71	3,208,110	0.067	128,030.34	0.490
5	14	4	220	4415.32	2,202,090	0.070	92,556.30	0.448
6	14	5	200	4514.94	2,354,290	0.067	94,286.20	0.445
7	14	6	260	4693.83	3,495,660	0.063	116,734.40	0.420
8	14	7	240	4798.00	3,447,750	0.061	110,576.50	0.426
9	15	4	240	4669.56	2,267,900	0.067	90,899.90	0.521
10	15	5	260	4806.95	3,369,870	0.065	115,508.20	0.504
11	15	6	200	4860.96	3,626,310	0.063	112,863.40	0.471
12	15	7	220	5008.76	3,656,210	0.061	109,058.00	0.493
13	16	4	260	4920.06	2,435,650	0.065	89,656.30	0.592
14	16	5	240	5030.26	2,395,300	0.062	91,386.60	0.624
15	16	6	220	5128.84	2,418,970	0.060	91,136.70	0.643
16	16	7	200	5220.97	2,402,330	0.059	86,735.70	0.663

The design variables, constraints, and objective functions presented above have been consolidated, and the mathematical model for optimizing the crashworthiness of the hull structure under a single working condition is formulated in Equation (27):

$$\begin{aligned}
 \min \quad & F = \alpha_M \cdot f(M) + \alpha_D \cdot f(D) - \alpha_P \cdot f(P) + \alpha_E \cdot f(E) \\
 \text{s.t.} \quad & 13 \text{ mm} \leq t_w \leq 16 \text{ mm} \\
 & 4 \text{ mm} \leq t_f \leq 7 \text{ mm} \\
 & 200 \text{ mm} \leq h \leq 260 \text{ mm} \\
 & m \leq 4860.96 \text{ kg}
 \end{aligned} \tag{27}$$

Taking into account the crashworthiness optimization problem under multi-working conditions with different collision positions, the mathematical model can be represented by Equation (28):

$$\begin{aligned}
 \min \quad & F(\mathbf{X}) = \sum_{i=1}^n \omega_i \cdot [W_1 \cdot |f_{i1}(\mathbf{X}) - f_{i1}^*(\mathbf{X})| + W_2 \cdot |f_{i2}(\mathbf{X}) - f_{i2}^*(\mathbf{X})|] \\
 \text{s.t.} \quad & 13 \text{ mm} \leq t_w \leq 16 \text{ mm} \\
 & 4 \text{ mm} \leq t_f \leq 7 \text{ mm} \\
 & 200 \text{ mm} \leq h \leq 260 \text{ mm} \\
 & m \leq 4860.96 \text{ kg}
 \end{aligned} \tag{28}$$

3.2. Orthogonal Design Samples

To address the multi-working condition crashworthiness optimization problem examined in this paper while considering the rationality of the orthogonal table design and structural manufacturability, the $L_{16} (4^5)$ orthogonal table was adopted for orthogonal design. The factors considered in the design were the thickness of the shell plating, the thickness of the frame web, and the height of the frame web, with each factor having four levels in the design domain. Specifically, the thickness of the shell plating had levels of 13 mm, 14 mm, 15 mm, and 16 mm; the thickness of the frame web had levels of 4 mm, 5 mm, 6 mm, and 7 mm; and the frame web height had levels of 200 mm, 220 mm, 240 mm, and 260 mm.

The response results (weight, peak collision force, collision depth, plastic energy absorption) of all sample points within the orthogonal table were calculated sequentially using the ABAQUS finite element software, with the results presented in Tables 2 and 3.

3.3. Training of BPNN Surrogate Model

Based on the predetermined parameters of the BPNN, BPNN surrogate models were constructed for two collision working conditions using Tables 2 and 3, respectively. In these models, the input layer has three nodes, the hidden layer has seven nodes, and the output layer has four nodes. The genetic algorithm iteration plot for Condition 1 is shown in Figure 9a, and the corresponding loss function curve for the BPNN is shown in Figure 9b. Similarly, the genetic algorithm iteration plot for Condition 2 is shown in Figure 10a, and the associated loss function curve for the BP neural network is shown in Figure 10b.

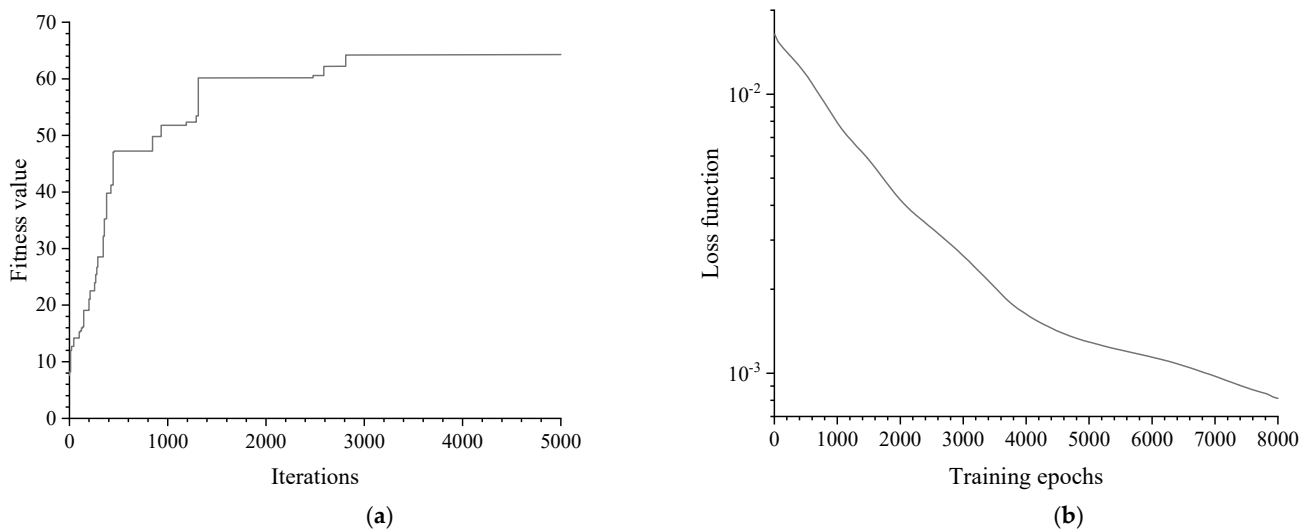


Figure 9. (a) Genetic algorithm iteration plot (Condition 1); (b) loss function curve for the BPNN (Condition 1).

From the GA fitness curve, it can be observed that the optimal fitness value changes dramatically in the early stage of algorithm iteration and does not have significant changes in the later stage. This is because the optimization objective of GA is the numerical minimal BP neural network error, which theoretically can only approach the optimal value of 0 indefinitely, and there is no truly minimal point. Therefore, when the iteration number is not set, GA will continue to optimize indefinitely, but the fitness value will become

increasingly flat with the increase of the iteration number. From the BP loss function curve, it can be seen that the network converges to an accuracy of nearly 10^{-3} after 8000 training iterations, and it only takes 2 s, indicating that the BP neural network in this paper is excellent in both training accuracy and efficiency.

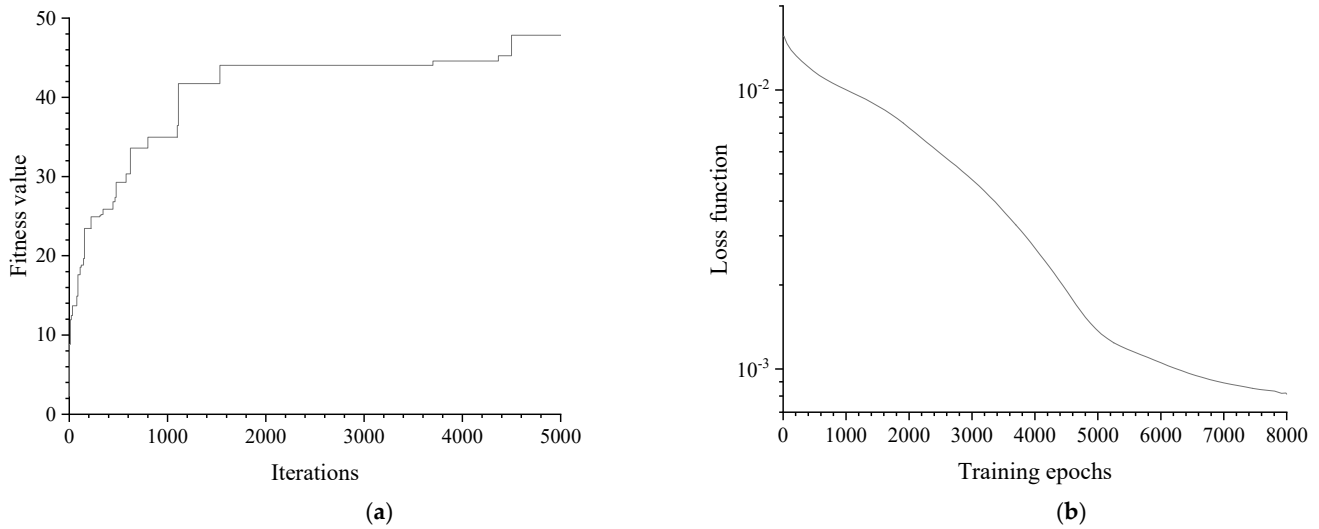


Figure 10. (a) Genetic algorithm iteration plot (Condition 2); (b) loss function curve for the BPNN (Condition 2).

3.4. Optimal Results

The two BPNN surrogate models established in the previous section are employed in optimization to provide effective predicted values for the objective function (Equation (28)) in the multi-working condition optimization. The ideal points for each optimization objective in Equation (28) are obtained through single-objective optimization using SSA based on the optimization objectives in Equation (27). By employing SSA, each crashworthiness index for individual working conditions is optimized separately, enabling the attainment of the optimal value for each index. In the sparrow search algorithm configuration, the population size is set at 100, with 20% dedicated to explorers and 10% to investigators. The security value is 0.8, and the number of iterations is 500. Subsequently, the obtained ideal points are substituted into Equation (28), and the sparrow search algorithm is employed once again to optimize the calculation, resulting in optimized outcomes for multiple working conditions. The convergence curve of the optimization process is shown in Figure 11.

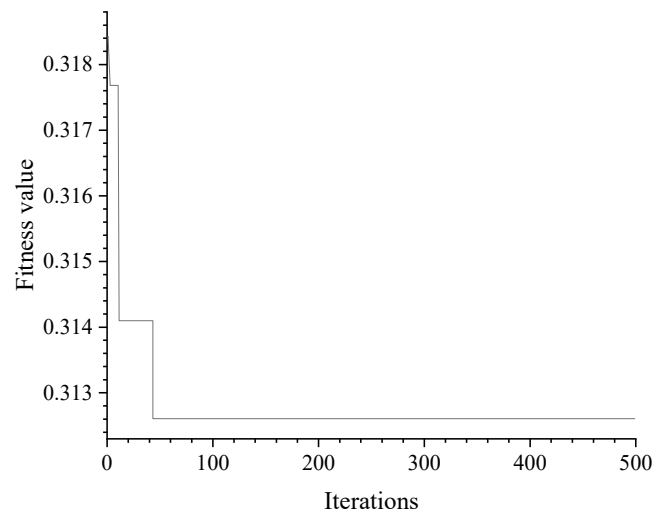


Figure 11. SSA iteration plot.

The output of the optimization yields the following results: the shell plating thickness is 13 mm, the frame web thickness is 5.36 mm, and the frame web height is 200 mm.

Compared to the predictive results of BPNN, the simulated values obtained through finite element calculations are more realistic. Therefore, this paper further utilizes ABAQUS finite element software to simulate and calculate the optimized results, while also validating the generalization ability of the BPNN. Tables 4 and 5 present the comparative results between the BPNN predicted values and the finite element simulated values under two collision conditions.

Table 4. Comparison between predicted and simulated values for Condition 1.

	Weight/kg	Peak Collision Force/(N)	Collision Depth/(m)	Plastic Energy Absorption/(J)
Predicted values	4339.19	2,535,273	0.075	121,148.98
Simulated values	4317.80	2,689,010	0.072	122,891.17
Relative error (%)	0.50	5.72	4.17	1.42

Table 5. Comparison between predicted and simulated values for Condition 2.

	Weight/kg	Peak Collision Force/(N)	Collision Depth/(m)	Plastic Energy Absorption/(J)
Predicted values	4351.93	3,386,878	0.069	117,932.80
Simulated values	4317.80	3,619,960	0.069	118,838.70
Relative error (%)	0.79	6.44	0	0.76

Based on the comparative results, the modified BPNN model showcased remarkable predictive accuracy in this paper, as evidenced by the minimal relative errors observed for various performance indicators under two collision conditions. For Condition 1, the relative errors ranged from 0.5% to 5.72% for different indicators, while for Condition 2, the relative errors ranged from 0.79% to 6.44% for different indicators. Notably, a perfect prediction (0% error) was achieved for one indicator in Condition 2. These findings unequivocally demonstrate the superior predictive efficacy and strong generalization capability of the modified BPNN model proposed in this paper. Such remarkable performance underscores the model’s potential for reliable predictions and highlights its suitability for practical applications in the field of ship collision. It can effectively replace laborious and time-consuming finite element calculations during the optimization process of the sparrow search algorithm.

To highlight the effectiveness of multi-working condition optimization, a comparison is made between the optimization results of multi-working condition optimization and the separate optimization results of two collision conditions, as shown in Table 6. In this table, “Optimization Condition” refers to the working condition currently used for optimization, and “Calculation Condition” refers to the working condition for which the optimization results are calculated using the optimized conditions.

Table 6. Comparing optimization results.

Optimization Condition	Calculation Condition	Thickness of the Shell Plating/(mm)	Thickness of the Frame Web/(mm)	Height of the Frame Web/(mm)	Weight/kg	Peak Collision Force/(N)	Collision Depth/(m)	Plastic Energy Absorption/(J)	Objective Function Value
Original design	Condition 1	13	6	240	4437.30	2,640,630	0.075	128,236.35	0.416
	Condition 2	13	6	240	4437.30	3,533,160	0.066	118,995.62	0.336
Condition 1	Condition 1	13	4	260	4204.80	2,681,300	0.079	123,571.30	0.313
	Condition 2	13	4	260	4204.80	3,231,880	0.073	118,193.30	0.340
Condition 2	Condition 1	13	5	220	4295.25	2,651,900	0.079	123,713.37	0.368
	Condition 2	13	5	220	4295.25	3,644,950	0.069	120,226.3	0.292
Multi-conditions	Condition 1	13	5.36	200	4317.80	2,689,010	0.072	122,891.17	0.287
	Condition 2	13	5.36	200	4317.80	3,619,960	0.069	118,838.70	0.301

From the calculated results of different optimization conditions in Table 6, it can be observed that compared to Condition 1 (collision area at the center of the plate), Condition 2 (collision area at the intersection of the plate and frame) experiences significantly higher collision force, but with less collision depth and plastic energy absorption. This indicates that the structural strength is higher at the intersection of the plate and frame compared to the center of the plate, highlighting the need to focus on the collision performance of Condition 1. However, in actual ship collision accidents, the collision area exhibits a certain level of randomness, so the collision performance of other areas (such as Condition 2) should not be overlooked.

The table presents the structural response when optimizing Condition 1 independently and calculating the results for Condition 2 based on the optimization results of Condition 1, as well as the structural response when optimizing Condition 2 independently and calculating the results for Condition 1 based on the optimization results of Condition 2. From these comparative results, it can be observed that when only pursuing the collision performance of Condition 1, the collision performance of Condition 2 is inferior to that achieved through the separate optimization of Condition 2, with objective function values of 0.34 and 0.292, respectively. Similarly, when only pursuing the collision performance of Condition 2, the collision performance of Condition 1 is also inferior to that achieved through the separate optimization of Condition 1, with objective function values of 0.368 and 0.313, respectively.

Therefore, in order to find a relative balance between the two conditions, this paper performed joint optimization considering multi-working conditions. By comparing the objective function of multi-working condition optimization with the objective functions of separate optimization for Condition 1 and Condition 2, it can be observed that the objective function values for Condition 1 in the multi-working condition optimization are smaller than the objective functions obtained from separate optimizations of Condition 1 and Condition 2: $0.287 < 0.313 < 0.368$. On the other hand, the objective function values for Condition 2 in the multi-working condition optimization fall between the objective function values obtained from separate optimizations of Condition 1 and Condition 2: $0.292 < 0.301 < 0.34$. This indicates that in the multi-working condition optimization approach presented in this paper, by considering both collision conditions simultaneously, the optimal solution can meet the relative optimality under both collision conditions. Moreover, the objective functions of Condition 1 and Condition 2 are significantly lower than the original design, with a reduction of 31% for Condition 1 and 10.4% for Condition 2, demonstrating excellent optimization results.

In terms of changes in structural dimensions, it can be concluded that maintaining the same shell plating thickness while appropriately increasing the thickness of the frame web and reducing its height contributes to improving the structural collision performance.

4. Discussion

4.1. Analysis of Improvement in BPNN

In order to analyze the learning ability of the modified BPNN on samples more intuitively, the modified BPNN is trained and compared with the original BPNN using sample data from two collision conditions. The comparative results are shown in Figure 12.

From Figure 12, it can be observed that when the preset accuracy is 10^{-4} , regardless of the collision conditions, the original BPNN fails to reach the preset accuracy within the specified number of training iterations. This indicates that the training efficiency of the BPNN based on the traditional gradient descent method is low, particularly when the learning rate is small, leading to slow convergence. On the other hand, the modified BPNN, which incorporates adaptive learning rate adjustment, is able to converge to the preset accuracy in fewer training iterations. Furthermore, compared to the original BPNN, the modified BPNN achieves a smaller loss value, indicating that the genetic algorithm (GA) can help the traditional BP neural network model escape local optima traps and enhance the model's learning ability. Consequently, after the modification, the BPNN exhibits significant improvements in both training accuracy and convergence speed.

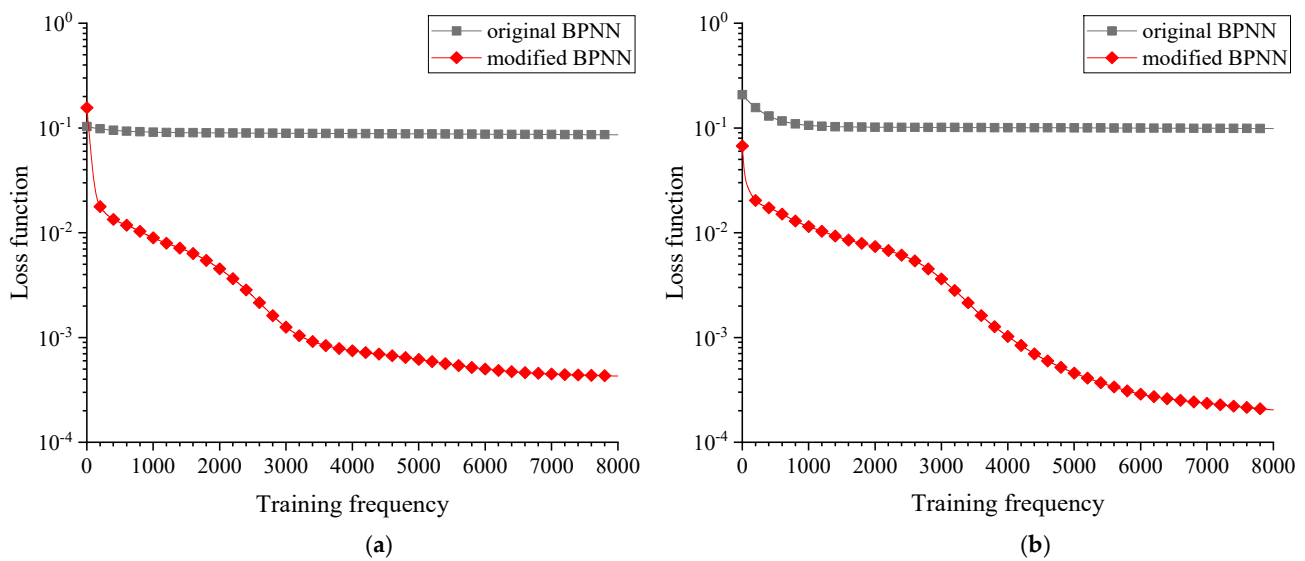


Figure 12. (a) Comparative results of BPNN before and after modification (Condition 1); (b) comparative results of BPNN before and after modification (Condition 2).

4.2. Analysis of Ship Crashworthiness Performance before and after Optimization

This paper aims to achieve relative optimality among various collision resistance indicators by considering the influence of multiple structural responses on structural crashworthiness during multi-objective optimization.

From the optimization results in Table 6, it can be observed that the total plastic energy absorption of the optimized structure has been reduced in both collision conditions, with percentage reductions of 4.16% and 0.14%, respectively. This indicates a decrease in the plastic deformation occurring in the collided region of the struck ship's structure. Regarding the peak collision forces, the optimized structure shows improvements compared to the original structure in both collision conditions, with increases of 1.80% and 2.40%, respectively. This suggests an enhanced ability of the optimized structure to withstand collision loads.

As for the parameter of maximum collision depth in the struck ship's hull structure, the optimized structure exhibits a 4.00% reduction under Condition 1. Although there is a 4.55% increase in the maximum collision depth of the optimized structure under Condition 2, when considering multiple weighted collision resistance indicators, the final objective function shows a decrease.

Figure 13 presents the damage deformation contour maps of the struck ship before and after optimization in two collision conditions. For the purpose of comparison, in this paper, a critical value of 150 MPa is set in the post-processing module of ABAQUS. The structural regions with stress levels below 150 MPa are represented in gray, while the regions with stress levels above 150 MPa are displayed with a continuous color gradient ranging from red to blue, corresponding to the magnitude of stress. By comparing the areas of the colored regions, it can be observed that the optimized structure has a smaller area of high-stress regions compared to the structure before optimization.

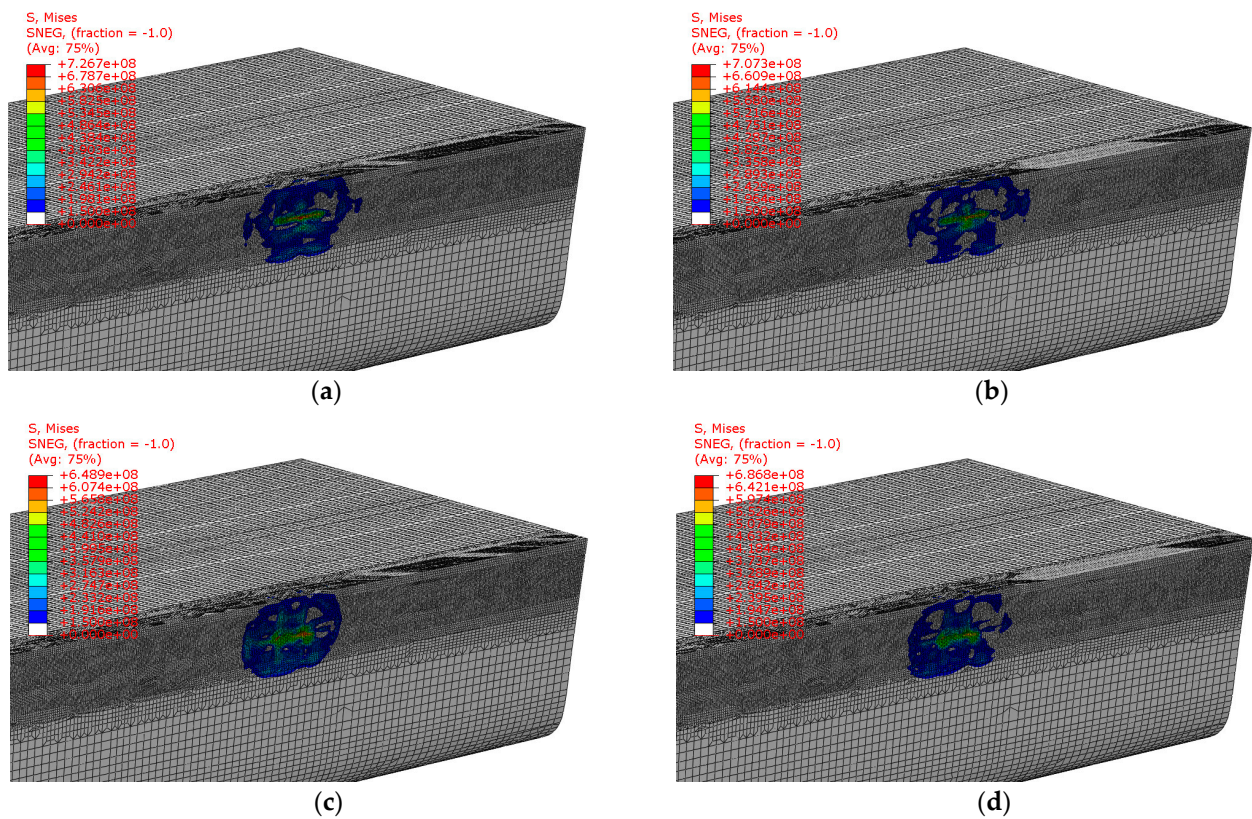


Figure 13. (a) Before optimization (Condition 1); (b) after optimization (Condition 1); (c) before optimization (Condition 2); (d) after optimization (Condition 2).

5. Conclusions

This paper presents a multi-working condition structural optimization design method, called BP-TSSA, based on BPNN, TOPSIS, and SSA, with the objective of enhancing the collision resistance performance of ship structures. The proposed method achieves significant improvements in the structural collision resistance performance compared to the original structure, and it also enables the attainment of relatively optimal structural designs for two different collision conditions.

The main results are as follows:

1. For the multi-working condition collision optimization problem in two different collision conditions, the optimized objective functions using the BP-TSSA algorithm proposed in this paper show a reduction of 31% and 10.4%, respectively, compared to the original designs. This indicates that the BP-TSSA algorithm proposed in this paper achieves good results in handling multi-working condition, multi-objective, and multi-parameter collision optimization problems for ship structures, demonstrating its excellent optimization capability;
2. The optimized results of the BPNN prediction align well with the finite element simulation results. This demonstrates that the BPNN surrogate model proposed in this paper possesses sufficient generalization ability;
3. The objective function values obtained for both collision conditions in the multi-working condition optimization are very small. This indicates that the multi-working condition optimization method proposed in this paper achieves relative optimality between the two collision conditions by considering them simultaneously.

In conclusion, the optimization method proposed in this paper can effectively enhance the collision resistance performance and optimization efficiency of ship structures. It can serve as an optimization tool for further design of ship structures and contribute to improving maritime safety.

Author Contributions: Conceptualization, W.Q. and K.L.; methodology, W.Q.; software, W.Q.; formal analysis, H.L.; data curation, S.Z.; visualization, H.L.; writing—original draft, W.Q.; writing—review and editing, Z.G. and K.L.; supervision, K.L. and J.W. All authors have read and agreed to the published version of the manuscript.

Funding: This research was funded by the National Natural Science Foundation of China (Grant No. 52171311; Grant 52271279) and the Jiangsu Province Graduate Research and Practice Innovation Program Project under Grant SJCX22_1958.

Institutional Review Board Statement: Not applicable.

Informed Consent Statement: Not applicable.

Data Availability Statement: Not applicable.

Conflicts of Interest: The authors declare no conflict of interest.

References

- Fang, J.; Sun, G.; Qiu, N.; Kim, N.H.; Li, Q. On design optimization for structural crashworthiness and its state of the art. *Struct. Multidiscip. Optim.* **2017**, *55*, 1091–1119. [[CrossRef](#)]
- Jiang, P.; Zhou, Q.; Shao, X. *Surrogate Model-Based Engineering Design and Optimization*; Springer: Berlin/Heidelberg, Germany, 2020.
- Angione, C.; Silverman, E.; Yaneske, E. Using machine learning as a surrogate model for agent-based simulations. *PLoS ONE* **2022**, *17*, e0263150. [[CrossRef](#)] [[PubMed](#)]
- Cho, S.; Kim, M.; Lyu, B.; Moon, I. Optimization of an explosive waste incinerator via an artificial neural network surrogate model. *Chem. Eng. J.* **2021**, *407*, 126659. [[CrossRef](#)]
- Karsh, P.; Kumar, R.; Vaishali; Dey, S. Radial Basis Function-Based Uncertain Low-Velocity Impact Behavior Analysis of Functionally Graded Plates. In *Machine Learning Applied to Composite Materials*; Springer: Berlin/Heidelberg, Germany, 2022; pp. 77–97.
- Mao, L.; Zhu, X.; Huang, Z.; Li, Y. Shock response of composite lattice sandwich structure subjected to underwater explosion. *Chin. J. Ship Res.* **2022**, *17*, 253–263.
- Wei, Y.; Zhong, Q.; Wang, D. Ultimate strength prediction of I-core sandwich plate based on BP neural network. *Chin. J. Ship Res.* **2022**, *17*, 125–134.
- Peng, W.; Zhang, J.; Shi, M.; Li, J.; Guo, S. Low-frequency sound insulation optimisation design of membrane-type acoustic metamaterials based on Kriging surrogate model. *Mater. Des.* **2023**, *225*, 111491. [[CrossRef](#)]
- Lin, Y.; He, J.; Li, K. Hull form design optimization of twin-skeg fishing vessel for minimum resistance based on surrogate model. *Adv. Eng. Softw.* **2018**, *123*, 38–50. [[CrossRef](#)]
- Prebeg, P.; Andric, J.; Rudan, S.; Jambrecic, L. Multiobjective ship structural optimization using surrogate models of an oil tanker crashworthiness. In *Marine Design XIII*; CRC Press: Boca Raton, FL, USA, 2018; pp. 459–470.
- Chen, D.; Jing, L.; Yang, F. Optimal design of sandwich panels with layered-gradient aluminum foam cores under air-blast loading. *Compos. Part B Eng.* **2019**, *166*, 169–186. [[CrossRef](#)]
- Herranen, H.; Pabut, O.; Eerme, M.; Majak, J.; Pohlak, M.; Jaan, K.; Saarna, M.; Allikas, G.; Aruniit, A. Design and testing of sandwich structures with different core materials. *Mater. Sci.* **2012**, *18*, 45–50. [[CrossRef](#)]
- Jiang, Z.; Gu, M. Optimization of a fender structure for the crashworthiness design. *Mater. Des.* **2010**, *31*, 1085–1095. [[CrossRef](#)]
- Ali, T.; Peng, Y.; Jinhao, Z.; Kun, L.; Renchuan, Y. Crashworthiness optimization method for sandwich plate structure under impact loading. *Ocean Eng.* **2022**, *250*, 110870. [[CrossRef](#)]
- Yan, J.; Li, L. Multi-objective optimization of milling parameters—the trade-offs between energy, production rate and cutting quality. *J. Clean. Prod.* **2013**, *52*, 462–471. [[CrossRef](#)]
- Ke, L.; Liu, K.; Wu, G.; Wang, Z.; Wang, P. Multi-objective optimization design of corrugated steel sandwich panel for impact resistance. *Metals* **2021**, *11*, 1378. [[CrossRef](#)]
- Liu, Z.; Lu, J.; Zhu, P. Lightweight design of automotive composite bumper system using modified particle swarm optimizer. *Compos. Struct.* **2016**, *140*, 630–643. [[CrossRef](#)]
- Li, Y.; Yang, Q.; Chang, T.; Qin, T.; Wu, F. Multi-load cases topological optimization by weighted sum method based on load case severity degree and ideality. *Adv. Mech. Eng.* **2020**, *12*, 1687814020947510. [[CrossRef](#)]
- Bo, L.; Zhang, M.; Hanyu, L.; Hong, N. Optimization design containing dimension and buffer parameters of landing legs for reusable landing vehicle. *Chin. J. Aeronaut.* **2022**, *35*, 234–249.
- Deb, K.; Deb, K. Multi-objective optimization. In *Search Methodologies: Introductory Tutorials in Optimization and Decision Support Techniques*; Springer: Berlin/Heidelberg, Germany, 2013; pp. 403–449.
- Stanimirovic, I.P.; Zlatanovic, M.L.; Petkovic, M.D. On the linear weighted sum method for multi-objective optimization. *Facta Acta Univ.* **2011**, *26*, 49–63.

22. Chiley, V.; Sharapov, I.; Kosson, A.; Koster, U.; Reece, R.; Samaniego de la Fuente, S.; Subbiah, V.; James, M. Online normalization for training neural networks. *Adv. Neural Inf. Process. Syst.* **2019**, *32*, 8433–8443.
23. Smith, A.E.; Coit, D.W.; Baeck, T.; Fogel, D.; Michalewicz, Z. Penalty functions. *Handb. Evol. Comput.* **1997**, *97*, C5.
24. Yoon, K.P.; Hwang, C.-L. *Multiple Attribute Decision Making: An Introduction*; Sage Publications: New Delhi, India; Thousand Oaks, CA, USA; London, UK, 1995.
25. Su, L.; Zhang, J.; Wang, C.; Zhang, Y.; Li, Z.; Song, Y.; Jin, T.; Ma, Z. Identifying main factors of capacity fading in lithium ion cells using orthogonal design of experiments. *Appl. Energy* **2016**, *163*, 201–210. [[CrossRef](#)]
26. Rumelhart, D.E.; Hinton, G.E.; Williams, R.J. *Learning Internal Representations by Error Propagation*; California University San Diego La Jolla Institute for Cognitive Science: La Jolla, CA, USA, 1985.
27. Sampson, J.R. Adaptation in natural and artificial systems (John H. Holland). *SIAM Rev.* **1976**, *18*, 529–530. [[CrossRef](#)]
28. Kingma, D.P.; Ba, J. Adam: A method for stochastic optimization. *arXiv* **2014**, arXiv:1412.6980.
29. Xue, J.; Shen, B. A novel swarm intelligence optimization approach: Sparrow search algorithm. *Syst. Sci. Control Eng.* **2020**, *8*, 22–34. [[CrossRef](#)]
30. Yan, S.; Yang, P.; Zhu, D.; Zheng, W.; Wu, F. Improved sparrow search algorithm based on iterative local search. *Comput. Intell. Neurosci.* **2021**, *2021*, 6860503. [[CrossRef](#)] [[PubMed](#)]
31. Chen, H.; Li, W.; Yang, X. A whale optimization algorithm with chaos mechanism based on quasi-opposition for global optimization problems. *Expert Syst. Appl.* **2020**, *158*, 113612. [[CrossRef](#)]
32. Meng, X.-B.; Gao, X.Z.; Lu, L.; Liu, Y.; Zhang, H. A new bio-inspired optimisation algorithm: Bird Swarm Algorithm. *J. Exp. Theor. Artif. Intell.* **2016**, *28*, 673–687. [[CrossRef](#)]
33. Reynolds, A. Liberating Lévy walk research from the shackles of optimal foraging. *Phys. Life Rev.* **2015**, *14*, 59–83. [[CrossRef](#)]
34. Jones, N. Some comments on the modelling of material properties for dynamic structural plasticity. *Mech. Prop. Mater. High Rates Strain* **1989**, *102*, 435–445.
35. Jones, N. *Structural Impact*; Cambridge University Press: Cambridge, UK, 2011.
36. Minorsky, V. *An Analysis of Ship Collisions with Reference to Protection of Nuclear Power Plants*; Sharp (George G.) Inc.: New York, NY, USA, 1958.

Disclaimer/Publisher’s Note: The statements, opinions and data contained in all publications are solely those of the individual author(s) and contributor(s) and not of MDPI and/or the editor(s). MDPI and/or the editor(s) disclaim responsibility for any injury to people or property resulting from any ideas, methods, instructions or products referred to in the content.